

See discussions, stats, and author profiles for this publication at: <https://www.researchgate.net/publication/45649861>

# NMR Structure of the SARS-CoV Nonstructural Protein 7 in Solution at pH6.5

ARTICLE in JOURNAL OF MOLECULAR BIOLOGY · OCTOBER 2010

Impact Factor: 4.33 · DOI: 10.1016/j.jmb.2010.07.043 · Source: PubMed

---

CITATIONS

7

---

READS

23

3 AUTHORS, INCLUDING:



**Kristaps Jaudzems**

Latvian Institute of Organic Synthesis

23 PUBLICATIONS 179 CITATIONS

SEE PROFILE



**Kurt Wüthrich**

The Scripps Research Institute

742 PUBLICATIONS 75,324 CITATIONS

SEE PROFILE

Published in final edited form as:

*J Mol Biol.* 2010 October 1; 402(4): 619–628. doi:10.1016/j.jmb.2010.07.043.

## NMR Structure of the SARS Coronavirus Nonstructural Protein 7 in Solution at pH 6.5

Margaret A. Johnson<sup>a</sup>, Kristaps Jaudzems<sup>a</sup>, and Kurt Wüthrich<sup>a,b,c,\*</sup>

<sup>a</sup>Department of Molecular Biology The Scripps Research Institute, La Jolla, CA 92037, USA

<sup>b</sup>Department of Chemistry, The Scripps Research Institute, La Jolla, CA 92037, USA

<sup>c</sup>The Skaggs Institute for Chemical Biology, The Scripps Research Institute, La Jolla, CA 92037, USA

### Abstract

The NMR structure of the severe acute respiratory syndrome coronavirus (SARS-CoV) non-structural protein 7 (nsp7) in aqueous solution at pH 6.5 was determined and compared with the results of previous structure determinations of nsp7 in solution at pH 7.5 and in crystals of a hexadecameric nsp7/nsp8 complex obtained from a solution at pH 7.5. All three structures contain four helices as the only regular secondary structures, but there are differences in the lengths and sequence locations of the four helices, as well as between the tertiary folds. The present study includes data on conformational equilibria and intramolecular rate processes in nsp7 in solution at pH 6.5, which provides further insights into the polymorphisms implicated by comparison of the presently available three nsp7 structures.

### Keywords

severe acute respiratory syndrome (SARS); coronavirus; nsp7; NMR structure; conformational polymorphism

### Introduction

The severe acute respiratory syndrome coronavirus (SARS-CoV) nonstructural protein 7 (nsp7) is of interest for its potential roles in the transcription and replication of the positive-stranded viral RNA genome. The four proteins nsp7 to nsp10, which are conserved among all CoVs but have no functional homologs outside of the *Coronaviridae*, are translated as part of the viral polyproteins pp1a and pp1ab, and the mature proteins are released by the action of the SARS-CoV protease nsp5.<sup>1,2,3</sup> An important role of nsp7 is indicated by the observation that deletion of nsp7 or mutation of the nsp7/nsp8 proteolytic cleavage site is lethal in murine hepatitis virus (MHV).<sup>4</sup> The expression of nsp7 in infected cells has been demonstrated for viruses belonging to three of the major CoV phylogenetic groups, namely human coronavirus 229E (group I),<sup>5</sup> MHV (group II),<sup>6</sup> and avian infectious bronchitis virus

© 2010 Elsevier Ltd. All rights reserved

\*Corresponding Author: Prof. Kurt Wüthrich, Department of Molecular Biology, MB-44, The Scripps Research Institute, 10550 North Torrey Pines Rd., La Jolla, CA 92037, USA. Tel: 1-858-784-8011, Fax: 1-858-784-8014, wuthrich@scripps.edu..

**Publisher's Disclaimer:** This is a PDF file of an unedited manuscript that has been accepted for publication. As a service to our customers we are providing this early version of the manuscript. The manuscript will undergo copyediting, typesetting, and review of the resulting proof before it is published in its final citable form. Please note that during the production process errors may be discovered which could affect the content, and all legal disclaimers that apply to the journal pertain.

(group III)<sup>7</sup>. During infection, nsp7 localizes to membrane-related sites of viral replication in the cytoplasm,<sup>5,6,8</sup> and in MHV it has been shown to interact specifically with nsp1 and nsp10 at sites of viral RNA synthesis.<sup>8</sup>

To provide a structural basis for functional studies, an NMR structure of nsp7 was determined in aqueous solution at pH 7.5,<sup>9</sup> and a crystal structure determination was reported<sup>10</sup> for a hetero-hexadecamer complex with nsp8, which has been shown to have RNA primase activity.<sup>11</sup> The complex in the crystal contains eight molecules each of nsp7 and nsp8 forming a channel with the appropriate width and charge to accommodate double-stranded RNA, and it was proposed to function as a potential processivity factor for RNA replication.<sup>10</sup> In both of these structures the polypeptide fold of nsp7 includes four helices as the only regular secondary structures, which cover approximately 60% of the 85-residue polypeptide chain. Comparison of the nsp7 folds in the two structures revealed extensive differences in the sequence positions and lengths of the four helices, as well as in the spatial arrangement of the helices in the tertiary structure. Interestingly, both structure determinations led to the conclusion, based on DALI searches,<sup>12,13</sup> that nsp7 represented a novel fold.<sup>9,10</sup>

In view of the implicated conformational polymorphism, and also considering that the NMR structure at pH 7.5 had to be calculated from a scarce set of experimental conformational constraints,<sup>9</sup> we decided to further investigate the behavior of nsp7 in different environments. The present project was therefore initiated by screening of a wide range of solution conditions in search of protein samples that would enable the recording of high-quality NMR data and the collection of more extensive sets of conformational constraints than had been possible at pH 7.5 and high ionic strengths.<sup>9</sup> Based on the results of this screen, an aqueous solution at pH 6.5 and low ionic strength was selected for a new NMR structure determination of nsp7. Additional NMR studies of conformational equilibria and dynamic processes further provided a foundation for rationalizing some aspects of the variations among the three now available nsp7 structures.

## Preparation of an nsp7 solution at pH 6.5

Nsp7 was expressed in *E. coli* BL21(DE3)-RIL cells using the plasmid pET28a with an N-terminal 6×His tag and a tobacco etch virus (TEV) protease cleavage site.<sup>9</sup> Two residues derived from the tag, Gly 1 and His 2, remained attached to the protein after purification. Uniformly <sup>15</sup>N- or [<sup>13</sup>C,<sup>15</sup>N]-labeled protein was produced by growth in M9 minimal medium containing 1 g/L of <sup>15</sup>NH<sub>4</sub>Cl as the sole nitrogen source and 4 g/L of either unlabeled glucose or <sup>13</sup>C<sub>6</sub>-D-glucose as the sole carbon source. Cell cultures were grown at 37 °C with shaking to an optical density at 600 nm of ~0.6. The temperature was then lowered to 18 °C, expression was induced with 1 mM isopropyl-β-D-thiogalactopyranoside (IPTG), and the cultures were grown for a further 18 h.

Following collection of the cells and storage at –80 °C, the cell pellets were disrupted by sonication in lysis buffer (50 mM Tris at pH 8, 500 mM NaCl, 5 mM imidazole, 0.1% Triton X-100, 3.5 mM DTT and EDTA-free Complete protease inhibitors (Roche)). The solution was centrifuged to remove cell debris, filtered through a 0.22 μm syringe filter (Millipore), and the supernatant was applied to a 5 ml HisTrap Crude column (GE Life Sciences) equilibrated with buffer A (lysis buffer without detergent and protease inhibitors). The bound proteins were eluted with a gradient from 5 to 500 mM imidazole, concentrated and exchanged by ultrafiltration (Millipore Ultrafree centrifugal concentrators, molecular weight cutoff 3 kDa) into buffer A' (50 mM sodium phosphate at pH 7.5, 300 mM NaCl) containing 10 mM DTT. The solution was treated with TEV protease for 18 h at room temperature, and the cleaved protein was then eluted in the flow-through of a 5 ml HisTrap Crude column

equilibrated with buffer A' containing 4 mM DTT (since nsp7 oxidizes readily, freshly prepared buffers and the maximum DTT concentrations compatible with the column resins were used throughout the purification). The protein was again concentrated, filtered and further purified on a Superdex 75 26/60 column (GE Life Sciences) equilibrated with buffer A' containing 5 mM DTT. Finally, the protein was exchanged by ultrafiltration into 'NMR buffer' (50 mM sodium phosphate at pH 6.5, 150 mM NaCl). The NMR samples contained 2 mM nsp7, 10 mM DTT-d<sub>10</sub>, 7% D<sub>2</sub>O and 0.02% NaN<sub>3</sub> in a volume of 600  $\mu$ l.

## Structure and dynamics of nsp7 in solution at pH 6.5

NMR samples containing 2 mM nsp7 in 50 mM sodium phosphate buffer at pH 6.5 with 150 mM NaCl were used for the structure determination at 25°C. This choice was based on the results of a screen for high-quality NMR spectra in a wide range of buffers, pH-values and salt concentrations, using <sup>15</sup>N-labeled nsp7 and 1.7-mm microcoil NMR equipment at 700 MHz, and on circular dichroism measurements of the unfolding temperature.

Complete backbone and side chain assignments for nsp7 were obtained, except for <sup>15</sup>N $\delta$ 1, H $\delta$ 1 and <sup>15</sup>N $\epsilon$ 2 of the histidines, <sup>15</sup>N $\epsilon$  and H $\epsilon$  of the arginines, and all backbone <sup>13</sup>C'. The <sup>13</sup>C $\alpha$  chemical shifts showed that nsp7 at pH 6.5 is an  $\alpha$ -protein with four helices (Fig. 1a). Structure calculation then resulted in a high-quality NMR structure, as shown by the statistics for the final cycle of calculation (Table 1). The protein forms an antiparallel bundle of four helices (Fig. 2a and b). The polypeptide segment 1–10, which includes the tag-derived residues Gly 1 and His 2, forms a disordered tail leading to a short extended segment of residues 11–12, which packs against side chains of the helices  $\alpha$ 2 and  $\alpha$ 4. The helix  $\alpha$ 1 (residues 13–20) is linked by a well-defined loop of residues 21–28 with the helix  $\alpha$ 2 (residues 29–42). A short segment of non-regular secondary structure leads to helix  $\alpha$ 3 (residues 47–65), and a short loop connects to helix  $\alpha$ 4 (residues 70–82). Multiple structural homologs to the structure of Fig. 2, a and b, were identified by a DALI search of the PDB.<sup>12,13</sup> These structural similarities probably result from the broad distribution among protein families of the four-helix bundle as a folding motif, and it is unlikely that these structural homologs indicate previously undetected functional homologs of nsp7 outside the *Coronaviridae*. The protein was further characterized by chemical cross-linking (Fig. 2c), which showed that nsp7 is monomeric in solution, and by a steady-state <sup>15</sup>N{<sup>1</sup>H}-NOE experiment, which is sensitive to ps to ns timescale mobility of the polypeptide backbone. Increased sub-nanosecond mobility was evident for the N-terminal decapeptide segment and the C-terminal hexapeptide, which includes the last turn of helix  $\alpha$ 4 (Fig. 1b), whereas the data for residues 13–79 show that this central polypeptide segment forms a compact globular fold.

## Conformational equilibria in nsp7 solutions at pH 6.5

The amide <sup>1</sup>H/<sup>2</sup>H exchange rates in <sup>2</sup>H<sub>2</sub>O solutions of proteins that have been lyophilized from <sup>1</sup>H<sub>2</sub>O reflect the degree of protection of each proton by the protein secondary and tertiary structures. Protons that are involved in hydrogen bonds of regular secondary structures, or are otherwise sequestered from the solvent, experience lower rates of chemical exchange. Amide proton protection factors (Pf) are defined as  $\log(k_{in}/k_{ex})$ , where  $k_{ex}$  is the measured hydrogen/deuterium exchange rate constant, and  $k_{in}$  is the intrinsic <sup>1</sup>H/<sup>2</sup>H exchange rate constant for the same residue type when exposed to the solvent.<sup>14</sup> In nsp7 at pH 6.5, the helices  $\alpha$ 2 and  $\alpha$ 3 have the highest protection factors, followed by  $\alpha$ 1 and then by  $\alpha$ 4, and for the polypeptide segments with non-regular secondary structure the protection was too small to be measured with the standard approach used here (Fig. 1c). The lack of protection for the amide protons of the N-terminal tetradecapeptide is in line with the presence of a short  $\alpha$ 1 helix in the NMR structure (Figs. 1 and 2).

Of special interest is the behavior of the helix  $\alpha 4$ . The reduced  $\Delta\delta(^{13}\text{C}^\alpha)$  values of the residues 78 to 82, when compared to the other helical regions (Fig. 1a), and the comparatively low protection factors for the entire helix (Fig. 1c) indicate that there is a reduced population of  $\alpha 4$  in the NMR structure because of a dynamic equilibrium with unstructured, solvent-accessible conformations. The latter are apparently not manifested in the NOE-based NMR structure, due to the absence of short  $^1\text{H}$ - $^1\text{H}$  distances that would correspond to  $d_{\text{NN}}$ ,  $d_{\alpha\text{N}}(i, i+3)$  and  $d_{\alpha\beta}(i, i+3)$  in the helix.<sup>15</sup> Since subnanosecond timescale motion of the protein backbone was observed only for the C-terminal hexapeptide segment of the protein (Fig. 1b), there was an indication that the conformational equilibria involving helix  $\alpha 4$  are governed by slower motions. This indication was confirmed by a line shape analysis. The residues Ser 63 and Gln 65 near the C-terminal end of  $\alpha 3$ , Val 68 in the loop joining  $\alpha 3$  and  $\alpha 4$ , and Asn 71 and Leu 73 at the start of  $\alpha 4$  all exhibit pronounced line-broadening when compared with residues in molecular regions that are not directly affected by the rate processes involving  $\alpha 4$  (Fig. 3). This line broadening was more pronounced when the temperature was decreased from 308 K to 288 K, indicating that the exchange between  $\alpha 4$  and conformations with solvent-exposed amide groups approaches the fast rate limit on the chemical shift timescale at 308 K (millisecond to sub-millisecond timescale), such that a single averaged signal is seen at all temperatures in Fig. 3.

## Functional implications from the polymorphism of nsp7 structures in different environments

Overall, the present study confirms the indications from earlier work that the helices  $\alpha 2$  and  $\alpha 3$  form a conserved core of the nsp7 structure, with their lengths, positions and relative orientation being largely preserved in different environments, and with the helices  $\alpha 1$  and  $\alpha 4$  adopting quite different lengths, positions in the sequence, and relative orientations (Fig. 4). In addition, new information was obtained on the time-scale of conformational equilibria in the solution structure at pH 6.5. A closer look at the three now available nsp7 structures reveals that the crystal structure of the complex with nsp8 differs from the pH 6.5 solution structure primarily by a rotation of the helix  $\alpha 4$  away from the  $\alpha 2/\alpha 3$  core, and by helical folding of the polypeptide segment of residues 3–12 (Fig. 4a). The long helix  $\alpha 1$  in the crystal structure (Fig. 4c), which would not be compatible with the amide proton protection factors measured in solution at pH 6.5 (Fig. 1c), then occupies the position taken by  $\alpha 4$  in the pH 6.5 solution structure (Fig. 4a). In the pH 7.5 solution structure,  $\alpha 4$  is packed against  $\alpha 3$  and has no contacts with  $\alpha 2$ , so that the three helices  $\alpha 2$ ,  $\alpha 3$  and  $\alpha 4$  line up to form a flat three-helix sheet (Fig. 4b), with  $\alpha 1$  packed at an angle of about  $45^\circ$  against  $\alpha 2$  and  $\alpha 3$ .

The nsp7 constructs used for the NMR studies and for the X-ray crystallographic studies included the expression tag-derived N-terminal elongations GH and GPLGS, respectively.<sup>9,10</sup> These tag-derived residues do not form part of the helix  $\alpha 1$  in any of the structures (Fig. 4c), and the tag-derived residues did not all give rise to clearly observable electron density in the crystal structure. These specific tag-residues are nonetheless of interest, since in the position preceding an  $\alpha$ -helix, both His and Ser have been observed to participate in helix-stabilizing N-capping interactions.<sup>16,17</sup> In two of the four nsp7 protomers in the crystal structure, hydrogen bonding between the side chain of the tag-derived Ser and helix  $\alpha 1$ , which might contribute to stabilizing a long helix  $\alpha 1$  in the crystals (Fig. 4c), is indeed possible. However, since the other two nsp7 protomers in the crystal do not display this interaction, and since the tag-derived residues are separated from  $\alpha 1$  by regions of non-regular secondary structure in solution, the tag-derived residues do not appear to have a dominant role with regard to the variable regular secondary structures seen under different conditions (Fig. 4).

Viral proteins can be exposed to significant pH changes as they move between different cellular compartments during viral infection, and therefore pH-dependent structure variations at near-physiological conditions may be relevant in triggering different protein-protein interactions during viral replication. Coronavirus replication is known to occur in double-membrane vesicles derived from the rough endoplasmic reticulum (ER),<sup>18</sup> which has a pH of about 7.0,<sup>19</sup> or from the ER/Golgi intermediate compartment (ERGIC). In contrast, viral budding takes place not only in the ERGIC but also in the Golgi apparatus,<sup>20,21</sup> which has a pH of about 6.5.<sup>22</sup> The regulation, transport and assembly processes that are involved in the transition from genome replication to viral particle budding and particle maturation are not well understood,<sup>18</sup> and a pH-dependent conformational transition in one or more of the nonstructural proteins (most of which have not been found in mature viral particles<sup>23</sup>) could be an essential step in viral genome packaging. That the antimalarial drug chloroquine has activity against the SARS-CoV and other viruses, by mechanisms that include a pH increase of the normally acidic trans-Golgi network,<sup>24,25</sup> provides further indications for a role of pH in controlling viral infection.

In the case of nsp7, where neither of the two solution structures would be compatible with the nsp8-binding mode observed in the crystal structure, it is tempting to speculate that nsp8 binds to a transient form of nsp7 in which the helix  $\alpha 4$  is unfolded, as implied by the data of Figs. 1c and 3. The binding to nsp8 would trigger the formation of the short helix  $\alpha 4$  immediately after  $\alpha 3$ , as well as the formation of the long helix  $\alpha 1$  (Fig. 4c), which then takes up the position occupied by  $\alpha 4$  in the pH 6.5 solution structure (Fig. 4a). In the crystal structure the locations of  $\alpha 1$  and  $\alpha 4$  are stabilized by numerous contacts with hydrophobic side chains of nsp8, in addition to the intramolecular contacts within nsp7, and the residues 79–85 are structurally disordered, as evidenced by the lack of electron density. Conformational variability of  $\alpha 4$  was seen also in the complex with nsp8, since the different molecules in the asymmetric unit of the crystal structure have different orientations of the helix  $\alpha 4$ .<sup>10</sup> There is thus an indication that locking of the helix  $\alpha 4$  of nsp7 in a conformation preventing binding to nsp8 could impair the replication machinery of the virus, which might provide a lead for future drug design.

Interestingly, while the nsp7 sequence in the helices  $\alpha 1$  to  $\alpha 3$  is highly conserved among all the coronaviruses, the sequence of the helix  $\alpha 4$  is quite variable,<sup>9</sup> indicating that the nsp7 fold could be interpreted as a scaffold consisting of a three-helix bundle, with a fourth helix in equilibrium with transiently unfolded forms affecting species specificity of the physiological activity. Considering the transient unfolding of  $\alpha 4$  at pH 6.5, the scarce interactions of  $\alpha 4$  with the rest of the protein in the pH 7.5 solution structure, and the complete lack of such interactions in the crystal structure, we truncated nsp7 at the end of the helix  $\alpha 3$ . Constructs consisting of residues 1–65, 1–66, 1–67, 1–69, 1–70 and 1–72 all yielded partly folded, poorly soluble proteins that were not amenable to structure determination by NMR (M.D. Geralt, P. Serrano, M.A. Johnson and K. Wüthrich, unpublished data). Conformations of the type observed at pH 6.5 in which the helix  $\alpha 4$  associates intimately with the bulk of the protein thus seem to be essential for protein stability and folding, and hence for functional integrity of nsp7.

## Data bank depositions

The chemical shifts of nsp7 at pH 6.5 were deposited in the BioMagResBank (<http://www.bmrb.wisc.edu>) under the accession number **16981**. The atomic coordinates of the ensemble of 20 conformers representing the solution structure of nsp7 at pH 6.5 were deposited in the Protein Data Bank (<http://www.rcsb.org/pdb>) with the code **2KYS**.



## Acknowledgments

We thank Michael D. Geralt and Dr. Pedro Serrano for helpful discussions. This study was supported by the NIAID/NIH contract #HHSN266200400058C “Functional and Structural Proteomics of the SARS-CoV” (P.I. Dr. P. Kuhn), the Joint Center for Structural Genomics through the NIH/NIGMS grant #U54-GM074898 (P.I. Dr. I.A. Wilson), and a fellowship to KJ by the Latvian Institute of Organic Synthesis. Kurt Wüthrich is the Cecil H. and Ida M. Green Professor of Structural Biology at TSRI.

## References

1. Masters PS. The molecular biology of coronaviruses. *Adv. Virus Res.* 2006; 66:193–292. [PubMed: 16877062]
2. Prentice E, McAuliffe J, Lu X, Subbarao K, Denison MR. Identification and characterization of severe acute respiratory syndrome coronavirus replicase proteins. *J. Virol.* 2004; 78:9977–9986. [PubMed: 15331731]
3. Gorbalenya AE, Enjuanes L, Ziebuhr J, Snijder EJ. Nidovirales: evolving the largest RNA virus genome. *Virus Res.* 2006; 117:17–37. [PubMed: 16503362]
4. Deming DJ, Graham RL, Denison MR, Baric RS. Processing of open reading frame 1a replicase proteins nsp7 to nsp10 in murine hepatitis virus strain A59 replication. *J. Virol.* 2007; 81:10280–10291. [PubMed: 17634238]
5. Ziebuhr J, Siddell SG. Processing of the human coronavirus 229E replicase polyproteins by the virus-encoded 3C-like proteinase: identification of proteolytic products and cleavage sites common to pp1a and pp1ab. *J. Virol.* 1999; 73:177–185. [PubMed: 9847320]
6. Bost AG, Carnahan RH, Lu XT, Denison MR. Four proteins processed from the replicase gene polyprotein of mouse hepatitis virus colocalize in the cell periphery and adjacent to sites of virion assembly. *J. Virol.* 2000; 74:3379–3387. [PubMed: 10708455]
7. Ng LF, Xu HY, Liu DX. Further identification and characterization of products processed from the coronavirus avian infectious bronchitis virus (IBV) 1a polyprotein by the 3C-like proteinase. *Adv. Exp. Med. Biol.* 2001; 494:291–298. [PubMed: 11774483]
8. Brockway SM, Lu XT, Peters TR, Dermody TS, Denison MR. Intracellular localization and protein interactions of the gene 1 protein p28 during mouse hepatitis virus replication. *J. Virol.* 2004; 78:11551–11562. [PubMed: 15479796]
9. Peti W, Johnson MA, Herrmann T, Neuman BW, Buchmeier MJ, Nelson M, Joseph J, Page R, Stevens RC, Kuhn P, Wüthrich K. Structural genomics of the severe acute respiratory syndrome coronavirus: nuclear magnetic resonance structure of the protein nsP7. *J. Virol.* 2005; 79:12905–12913. [PubMed: 16188992]
10. Zhai Y, Sun F, Li X, Pang H, Xu X, Bartlam M, Rao Z. Insights into SARS-CoV transcription and replication from the structure of the nsp7-nsp8 hexadecamer. *Nat. Struct. Mol. Biol.* 2005; 12:980–986. [PubMed: 16228002]
11. Imbert I, Guillemot JC, Bourhis JM, Bussetta C, Coutard B, Egloff MP, Ferron F, Gorbalenya AE, Canard B. A second, non-canonical RNA-dependent RNA polymerase in SARS coronavirus. *EMBO J.* 2006; 25:4933–4942. [PubMed: 17024178]
12. Holm L, Sander C. Protein structure comparison by alignment of distance matrices. *J. Mol. Biol.* 1993; 233:123–138. [PubMed: 8377180]
13. Holm L, Sander C. Dali: a network tool for protein structure comparison. *Trends Biochem. Sci.* 1995; 20:478–480. [PubMed: 8578593]
14. Bai Y, Milne JS, Mayne L, Englander SW. Primary structure effects on peptide group hydrogen exchange. *Proteins.* 1993; 17:75–86. [PubMed: 8234246]
15. Wüthrich, K. *NMR of Proteins and Nucleic Acids.* Wiley; New York: 1986.
16. Davis RB Jr, Lecomte JT. A dynamic N-capping motif in cytochrome b5: evidence for a pH-controlled conformational switch. *Proteins.* 2006; 63:336–348. [PubMed: 16372350]
17. Aurora R, Rose GD. Helix capping. *Protein Sci.* 1998; 7:21–38. [PubMed: 9514257]
18. Perlman S, Netland J. Coronaviruses post-SARS: update on replication and pathogenesis. *Nat. Rev. Microbiol.* 2009; 7:439–450. [PubMed: 19430490]

19. Tian H, Klambt D, Jones AM. Auxin-binding protein 1 does not bind auxin within the endoplasmic reticulum despite this being the predominant subcellular location for this hormone receptor. *J. Biol. Chem.* 1995; 270:26962–26969. [PubMed: 7592943]
20. Stertz S, Reichelt M, Spiegel M, Kuri T, Martinez-Sobrido L, Garcia-Sastre A, Weber F, Kochs G. The intracellular sites of early replication and budding of SARS-coronavirus. *Virology.* 2007; 361:304–315. [PubMed: 17210170]
21. Salanueva JJ, Carrascosa JL, Risco C. Structural maturation of the transmissible gastroenteritis coronavirus. *J. Virol.* 1999; 73:7952–7964. [PubMed: 10482542]
22. Kim JH, Lingwood CA, Williams DB, Furuya W, Manolson MF, Grinstein S. Dynamic measurement of the pH of the Golgi complex in living cells using retrograde transport of the verotoxin receptor. *J. Cell Biol.* 1996; 134:1387–1399. [PubMed: 8830769]
23. Neuman BW, Joseph JS, Saikatendu KS, Serrano P, Chatterjee A, Johnson MA, Liao L, Klaus JP, Yates JR 3rd, Wüthrich K, Stevens RC, Buchmeier MJ, Kuhn P. Proteomics analysis unravels the functional repertoire of coronavirus nonstructural protein 3. *J. Virol.* 2008; 82:5279–5294. [PubMed: 18367524]
24. Keyaerts E, Vijgen L, Maes P, Neyts J, Van Ranst M. In vitro inhibition of severe acute respiratory syndrome coronavirus by chloroquine. *Biochem. Biophys. Res. Commun.* 2004; 323:264–268. [PubMed: 15351731]
25. Vincent MJ, Bergeron E, Benjannet S, Erickson BR, Rollin PE, Ksiazek TG, Seidah NG, Nichol ST. Chloroquine is a potent inhibitor of SARS coronavirus infection and spread. *Viol. J.* 2005; 2:69. [PubMed: 16115318]
26. Renner C, Schleicher M, Moroder L, Holak TA. Practical aspects of the 2D  $^{15}\text{N}\{-^1\text{H}\}$ -NOE experiment. *J. Biomol. NMR.* 2002; 23:23–33. [PubMed: 12061715]
27. Kay LE, Keifer P, Saarinen T. Pure absorption gradient enhanced heteronuclear single quantum correlation spectroscopy with improved sensitivity. *J. Am. Chem. Soc.* 1992; 114:10663–10665.
28. Koradi R, Billeter M, Wüthrich K. MOLMOL: a program for display and analysis of macromolecular structures. *J. Mol. Graph.* 1996; 14:51–55. [PubMed: 8744573]
29. Kabsch W, Sander C. Dictionary of protein secondary structure: pattern recognition of hydrogen-bonded and geometrical features. *Biopolymers.* 1983; 22:2577–2637. [PubMed: 6667333]
30. Sattler M, Schleucher J, Griesinger C. Heteronuclear multidimensional NMR experiments for the structure determination of proteins in solution employing pulsed field gradients. *Prog. Nucl. Magn. Reson. Spectrosc.* 1999; 34:93–158.
31. Fiorito F, Herrmann T, Damberger FF, Wüthrich K. Automated amino acid side-chain NMR assignment of proteins using  $^{13}\text{C}$ - and  $^{15}\text{N}$ -resolved 3D [ $^1\text{H}$ ,  $^1\text{H}$ ]-NOESY. *J. Biomol. NMR.* 2008; 42:23–33. [PubMed: 18709333]
32. Wishart DS, Bigam CG, Yao J, Abildgaard F, Dyson HJ, Oldfield E, Markley JL, Sykes BD.  $^1\text{H}$ ,  $^{13}\text{C}$  and  $^{15}\text{N}$  chemical shift referencing in biomolecular NMR. *J. Biomol. NMR.* 1995; 6:135–140. [PubMed: 8589602]
33. Herrmann T, Güntert P, Wüthrich K. Protein NMR structure determination with automated NOE-identification in the NOESY spectra using the new software ATNOS. *J. Biomol. NMR.* 2002; 24:171–189. [PubMed: 12522306]
34. Herrmann T, Güntert P, Wüthrich K. Protein NMR structure determination with automated NOE assignment using the new software CANDID and the torsion angle dynamics algorithm DYANA. *J. Mol. Biol.* 2002; 319:209–227. [PubMed: 12051947]
35. Güntert P, Mumenthaler C, Wüthrich K. Torsion angle dynamics for NMR structure calculation with the new program DYANA. *J. Mol. Biol.* 1997; 273:283–298. [PubMed: 9367762]
36. Spera S, Bax A. Empirical correlation between protein backbone conformation and  $\text{C}^\alpha$  and  $\text{C}^\beta$   $^{13}\text{C}$  nuclear magnetic resonance chemical shifts. *J. Am. Chem. Soc.* 1991; 113:5490–5492.
37. Luginbühl P, Szyperski T, Wüthrich K. Statistical basis for the use of  $^{13}\text{C}^\alpha$  chemical shifts in protein structure determination. *J. Magn. Reson. B.* 1995; 109:229–233.
38. Koradi R, Billeter M, Güntert P. Point-centered domain decomposition for parallel molecular dynamics simulation. *Comput. Phys. Commun.* 2000; 124:139–147.



39. Luginbühl P, Güntert P, Billeter M, Wüthrich K. The new program OPAL for molecular dynamics simulations and energy refinements of biological macromolecules. *J. Biomol. NMR.* 1996; 8:136–146. [PubMed: 8914272]
40. Cornell WD, Cieplak P, Bayly CI, Gould IR, Merz KM Jr. Ferguson DM, Spellmeyer DC, Fox T, Caldwell JW, Kollman PA. A second generation force field for the simulation of proteins, nucleic acids, and organic molecules. *J. Am. Chem. Soc.* 1995; 117:5179–5197.
41. Laskowski RA, MacArthur MW, Moss DS, Thornton JM. PROCHECK: a program to check the stereochemical quality of protein structures. *J. Appl. Crystallogr.* 1993; 26:283–291.

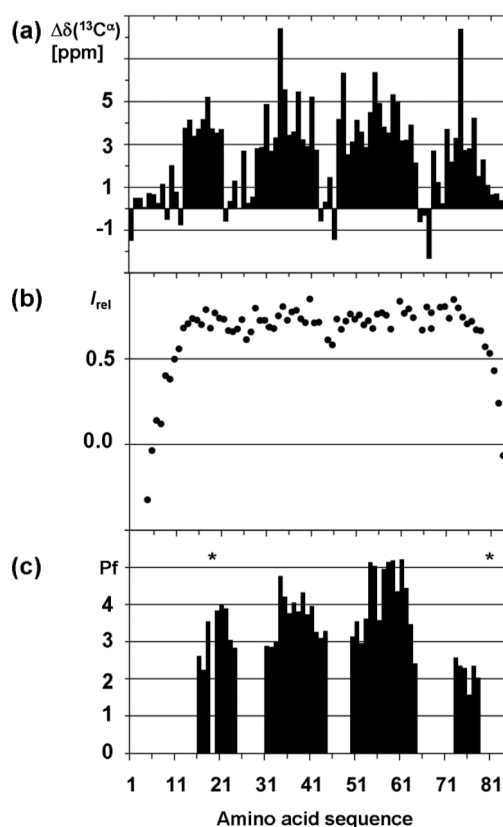


**Figure 1.**

Plots versus the amino acid sequence of nsp7 of NMR data measured in aqueous solution at pH = 6.5 and T = 25° C. (a)  $^{13}\text{C}^\alpha$  chemical shift deviations from random coil values,  $\Delta\delta(^{13}\text{C}^\alpha)$ . At the top the sequence locations of the four  $\alpha$ -helices are indicated. (b)  $^{15}\text{N}\{^1\text{H}\}$ -NOE values,  $I_{\text{rel}}$ , measured on a Bruker Avance 600 MHz spectrometer with a TCI z-gradient cryoprobe using sensitivity-enhanced experiments<sup>26,27</sup> with a saturation period of 3.0 s and a total interscan delay of 5.0 s. (c) Amide  $^1\text{H}/^2\text{H}$  exchange protection factors. The asterisks indicate positions where no measurements could be made due to spectral overlap. Pf values were determined using a 2 mM  $^{15}\text{N}$ -labeled protein sample that was lyophilized from  $^1\text{H}_2\text{O}$  solution and then redissolved in 99.9%  $^2\text{H}_2\text{O}$ . The decay of the signal intensity of the  $^{15}\text{N}$ - $^1\text{H}$  correlation peaks was monitored by acquiring a series of 2D [ $^{15}\text{N}$ ,  $^1\text{H}$ ]-HSQC spectra at different times after preparation of the  $^2\text{H}_2\text{O}$  solution. Each spectrum was acquired for 4 to 15 minutes, and the study was continued for 11 days. The peak intensities were fitted to an exponential equation of the form  $I = I_0 \exp(-k_{\text{ext}}t)$ , where we accounted for the residual peak intensities. Pf values were calculated taking into account the amino acid sequence effects on the random coil exchange rates (see text).

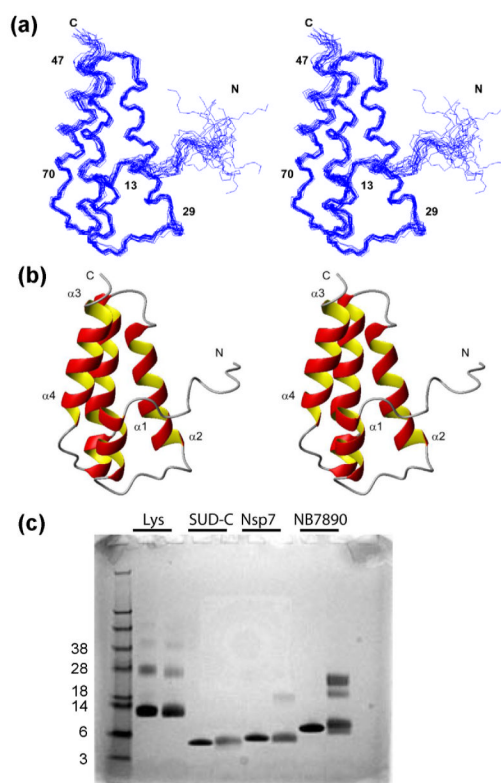


**Figure 2.**

Solution structure of nsp7 at pH 6.5. (a) Stereoview of a bundle of 20 energy-minimized conformers superimposed for minimal rmsd of the backbone atoms N, C $\alpha$  and C' of the residues 11–82. The chain ends and the start positions of each  $\alpha$ -helix are labeled. (b) Stereo-ribbon drawing of the conformer with minimal rmsd to the mean coordinates of the ensemble in (a). The chain ends are identified, and the  $\alpha$ -helices are labeled at their N-termini. (c) SDS-PAGE gel showing the results of an ethylene glycol bis[succinimidylsuccinate] (EGS) cross-linking experiment. The left margin shows molecular weight standards in kDa. The remaining four pairs of lanes show lysozyme (14.1 kDa), SUD-C (7.6 kDa), nsp7 (9.5 kDa) and NB7890 (11.6 kDa). Lysozyme and SUD-C are monomeric proteins, while NB7890 is a dimer. For each protein the left lane shows the control solution with no EGS added, and the right lane shows the result of the cross-linking reaction. The reactions were carried out with 50  $\mu$ M protein solutions at pH 7.3 and 5 mM EGS for 75 sec at room temperature, and stopped by adding Tris buffer at pH 8.0 to a concentration of 53 mM.

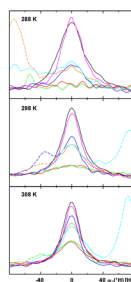


**Figure 3.**

Cross-sections along  $\omega_2$  ( $^1\text{H}$ ) from 2D [ $^{15}\text{N}$ ,  $^1\text{H}$ ]-HSQC spectra at 288 K, 298 K and 308 K, illustrating line broadening due to conformational exchange for the resonances of Ser 63 (red), Gln 65 (green), Val 68 (blue), Asn 71 (orange) and Leu 73 (cyan). The signals of Ala 32 (black) and Val 60 (magenta) are shown as references without exchange line broadening. Those parts of the cross-sections that are due to overlap with nearby peaks are drawn with dashed lines. The digital resolution is 2.0 Hz/point.

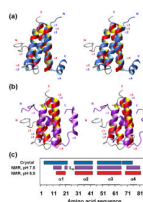


**Figure 4.**

Stereo-ribbon drawings of superpositions of the solution structure of nsp7 at pH 6.5 (red/yellow) with the two previously reported nsp7 structures, and sequence locations of the  $\alpha$ -helices in the three structures. (a) Superposition with the crystal structure of nsp7 in a complex with nsp8 (blue). (b) Superposition with the solution structure of nsp7 at pH 7.5 (purple). The structures were superimposed for minimal rmsd of the backbone N, C $^{\alpha}$  and C' atoms of the helices  $\alpha$ 2 and  $\alpha$ 3 (residues 29–42 and 47–65), which yielded rmsd values of 1.63 Å for (a) and 2.70 Å for (b) (the corresponding values for the superposition of the C $^{\alpha}$  atoms of the helices  $\alpha$ 2 and  $\alpha$ 3 were 1.77 Å for (a) and 2.91 Å for (b)). The chain ends and the starting positions of the helices are labeled with the respective colors. (c) Locations of  $\alpha$ -helices in the NMR structures determined at pH 6.5 and at pH 7.5,<sup>9</sup> and in the crystal structure of the complex with nsp8.<sup>10</sup> The numbering of the helices is indicated for the NMR structure at pH 6.5, and the color scheme is the same as in the panels (a) and (b). The locations of helices in the pH 7.5 solution structure were taken from reference 9. In the pH 6.5 solution structure, the locations of helices were determined by automatic analysis of the ensemble of 20 energy-minimized conformers (Fig. 2a) with the program MOLMOL,<sup>28</sup> which employs the algorithm of Kabsch and Sander<sup>29</sup> for secondary structure identification. Helix locations were assigned by determining the most common start- and end-points of each helix in the ensemble of conformers. The locations of helices in the crystal structure were determined by analysis of the coordinates (PDB accession code 2AHM<sup>10</sup>) with MOLMOL, using the second molecule in the asymmetric unit as the representative conformer.

**Table 1**

Input for the structure calculation and statistics of the ensemble of 20 energymimized CYANA conformers used to represent the NMR structure of nsp7 at pH = 6.5<sup>a</sup> and T = 25°C.

Quantity <sup>b</sup>	Value <sup>b</sup>
NOE upper distance limits <sup>a</sup>	2035
intraresidual	448
short-range	614
medium-range	599
long-range	374
Restraints/residue	28
Long-range restraints/residue	5
Dihedral angle constraints	382
Residual target function value (Å <sup>2</sup> )	1.95 ± 0.24
Residual NOE violations	
Number > 0.1 Å	36 ± 5
Maximum (Å)	0.15 ± 0.01
Residual dihedral angle violations	
Number > 2.5 °	1 ± 1
Maximum (°)	2.25 ± 1.45
Amber energies (kcal/mol)	
Total	-3264.44 ± 65.37
van der Waals	-217.35 ± 15.87
Electrostatic	-3725.29 ± 57.16
RMSD from ideal geometry	
Bond lengths (Å)	0.0078 ± 0.0002
Bond angles (°)	2.158 ± 0.072
RMSD to the mean coordinates (Å) <sup>c</sup>	
bb	0.46 ± 0.06 (11–82)
ha	0.82 ± 0.08 (11–82)
Ramachandran plot statistics (%) <sup>d</sup>	
Most favored regions	75.2
Additional allowed regions	20.7
Generously allowed regions	2.9
Disallowed regions	1.2

<sup>a</sup>The structure determination was based on a 3D <sup>15</sup>N-resolved [<sup>1</sup>H,<sup>1</sup>H]-NOESY spectrum with 100 ms mixing time and two 3D <sup>13</sup>C-resolved [<sup>1</sup>H,<sup>1</sup>H]-NOESY spectra with the carrier frequency centered in the aliphatic and aromatic carbon regions and with mixing times of 150 ms and 60



ms, respectively, recorded on a Bruker Avance 800 spectrometer with a TXI z-gradient probe. The protein backbone resonances were assigned based on 3D HNCA, 3D HNCACB and 3D CBCA(CO)NH experiments.<sup>30</sup> Automated side chain resonance assignment were based on using the three 3D NOESY data sets as input for the program ASCAN,<sup>31</sup> followed by interactive verification based on a 3D HC(C)H-TOCSY experiment. <sup>1</sup>H chemical shifts were referenced to internal 3-(trimethylsilyl)-1-propanesulfonic acid sodium salt (DSS). The <sup>13</sup>C and <sup>15</sup>N chemical shifts were referenced indirectly to DSS using the absolute frequency ratios.<sup>32</sup> Structure calculation used the three aforementioned NOESY data sets as input for the stand-alone program suite ATNOS/CANDID 2.233,<sup>34</sup> and the torsion angle molecular dynamics program CYANA 3.0.<sup>35</sup> Backbone  $\phi$  and  $\psi$  dihedral angle constraints derived from the <sup>13</sup>C $\alpha$  chemical shifts were used as supplementary data in the input.<sup>36,37</sup> In the seventh ATNOS/CANDID/CYANA cycle, 40 conformers were generated and subjected to energy minimization in a water shell with OPALp<sup>38,39</sup> using the AMBER force field,<sup>40</sup> and the 20 best energy-minimized conformers were selected to represent the solution structure. The program MOLMOL<sup>28</sup> was used for structure analysis and presentation. The stereochemical quality of the molecular models was analyzed using the Protein Data Bank validation server (<http://deposit.pdb.org/validate>).

<sup>b</sup> The top 8 entries describe the input from the NMR experiments. The other entries refer to the ensemble of 20 CYANA conformers after energy minimization with OPALp. The ranges indicate the standard deviations.

<sup>c</sup> <sub>bb</sub> indicates the backbone atoms N, C $\alpha$  and C'; ha stands for "all heavy atoms". The numbers in parentheses indicate the residues for which the RMSD was calculated.

<sup>d</sup> As determined by PROCHECK.<sup>41</sup>